Commercial Off-The-Shelf GMR Based Sensor on Board Optos Picosatellite

M.D. Michelena

Instituto Nacional de Técnica Aeroespacial (INTA),
28850 Madrid, Spain
diazma@inta.es

Abstract. Space is an environment of extreme parameters. Wide temperature swings, very low pressures (vacuum), moderate to high radiation, mechanical vibrations and impacts, etc. Thus, components for space applications, which need to stand these hard conditions, are normally very expensive and it often takes a while to include emerging technologies in the space market. This means that space components are not always that innovative.

The case of vector magnetometers is not an exception. Since the beginning of the space exploration mainly fluxgate magnetometers have been used for magnetic mapping [1]. Fluxgates are robust sensors and massive core fluxgates present very good performances for geomagnetic mapping and further exploration in the solar system. Besides, they are normally combined with a scalar absolute sensor for calibration of the vector magnetometer.

In an attempt to be able to get ready as fast as possible to use emerging magnetic sensing technologies for space applications, INTA has devoted some effort in the qualification for flight use, of Commercial Off-The-Shelf (COTS) solid state magnetic sensors, as AMR and GMR sensors [2-4].

In this chapter we describe the chain of testing and adaptation of the available commercial GMR sensors for an experimental payload in a picosatellite (OPTOS, 3 kg). We present the calibration tests results and the expectations we have for the in-orbit measurements.

1 Introduction – A Flight Opportunity

This chapter reports on the first GMR commercial sensor on board a satellite: from the conception to the preflight calibrations. The idea of such a challenge starts in 2005 encouraged by the increasing interest of GMR sensors mostly in recording magnetic heads [5-9]. The group of Space Magnetism of the Spanish National Institute of Aerospace Technology (INTA), born in the end of the nineties, defined its strategy with the upqualification of commercial off-the-shelf (COTS) magnetic sensors for space applications with the aim to be ready for the qualifications of the new emerging technologies [2]. In this line already in 2005 a miniaturized AMR-based sensor had been launched onboard NANOSAT-01, and the idea to broad this initiative to GMR

C. Reig et al.: *Giant Magnetoresistance (GMR) Sensors*, SSMI 6, pp. 181–210.
DOI: 10.1007/978-3-642-37172-1_8

sensors with half volume of an AMR, double response to magnetic field, and a potential lower power consumption, was very challenging.

At that time, three Spanish space missions started almost simultaneously:

1) An INTA picosatellite (mass lower than 3 kg) called OPTOS "A New Light in Space": a platform for technology experimentation [10]. Among the proposed payloads there were an optical camera APIS, an experiment to measure the temperature by means of a set of optical fibers (FIBOS), and we were asked to propose a magnetic experiment: a GMR-based experiment. Actually OPTOS had another AMR-based magnetometer onboard for the attitude and orbit control subsystem (AOCS), so the whole experiment consisted in the intercomparison of both vector sensors.

   OPTOS, composed of three piled cubesats [11-13], is a real challenge of compactness. Imagine how to place the computer, the power unit, etc. and several payloads in a volume of 10 cm x 10 cm x 30 cm. In this compact scenario, the communications between the computer and the rest of the units are performed by means of optical wireless links (OWLS). The wires are completely removed fundamentally to make it easier the integration and assembly tasks.
2) A second nanosatellite in the frame of NANOSAT program: NANOSAT-1B. A more advanced and experimented platform for technology demonstration. Onboard this platform the initial experimental payloads were a couple of magnetic sensors: the GMR and a magnetoimpedance vector, and an experiment for the measurement of the total radiation flux by means of the effect the radiation has in the dark current of optoelectronic devices: *Las Dos Torres* (The Two Towers) [14].
3) A national satellite for Earth observation: SEOSAT. This was supposed to be the first Spanish satellite with the capability to take high resolution multispectral images for different purposes like cartography, agricultural and aquifers mapping, catastrophes and security management, etc. Again, in this platform, two very small payloads were proposed: the Two Towers and a GMR vector sensor called MAGNETITA.

In the three space mission the scientific objective for the GMR sensors was to measure the geomagnetic field (± 60 μT) with accuracy in the order of 10 nT, which is a typical resolution for attitude determination not very strict.

Figure 1 shows the block diagram of the different experiments on board the three platforms. It can be seen that the more complex experiment was proposed for SEOSAT, and consisted in a couple of vector sensors for intercomparison, a calibration coil and a temperature sensor, for thermal compensation due to the high temperature dependence of solid state sensors, within the same experiment. Experiment for

NANOSAT-1B followed this one in complexity, with calibration coil and temperature sensor in the experiment and the open possibility to compare GMR measurements with the AMR sensor. Finally the experiment onboard OPTOS was very limited as a whole but again there were coils in the satellite for GMR calibration and the above mentioned AMR sensor for the AOCS. It can be seen how the complexity of the experiment was reduced as mass was more limited: SEOSAT mass is above 700 kg, NANOSAT-1B mass is 20 kg and OPTOS is less than 3 kg.

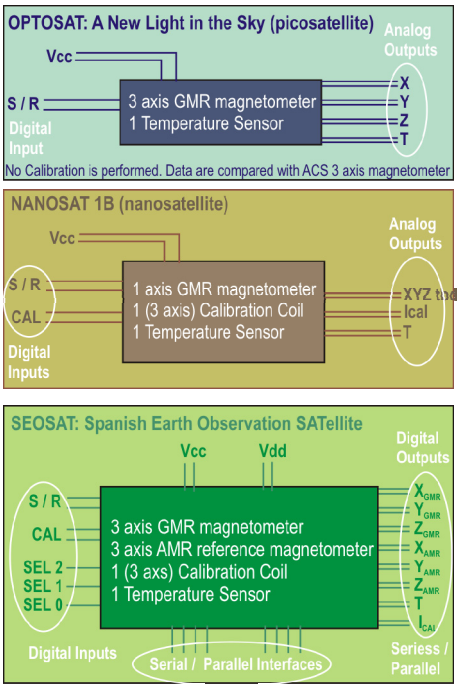

Fig. 1. Blocks diagram of the GMR experiments proposed for the three platforms

In 2006 NANOSAT-1B restricted the magnetic experimental payloads to one and then the magnetoimpedance experiment continued alone onboard this platform. In 2008 MAGNETITA also got off of SEOSAT so the GMR experiment onboard OPTOS is the only one that has survived up today and the protagonist of this story.

2 Selection of an Appropriate Commercial Off-The-Shelf (COTS) GMR Sensor

As it has been described previously in this book, GMR effect is the change in electrical resistance of a multilayer of ferromagneticaly coupled magnetic layers, separated by non magnetic layers, when it is exposed to a magnetic field. In this chapter it is only considered the group of sensors consisting of a multilayer of two ferromagnetic layers separated by a metallic layer (GMR). Other types of sensors like the Magnetic Tunnel Junctions (MTJs) consisting of a trilayer of ferromagnetic material with an inner insulator are not taken into consideration [15-16].

In the absence of a magnetic field the magnetization of the GMR above mentioned sensors, is perpendicular to the measuring axis and alternate among the layers. When a magnetic field is applied, the magnetization of the magnetic layers rotates towards the direction of the external magnetic field (Figure 2).

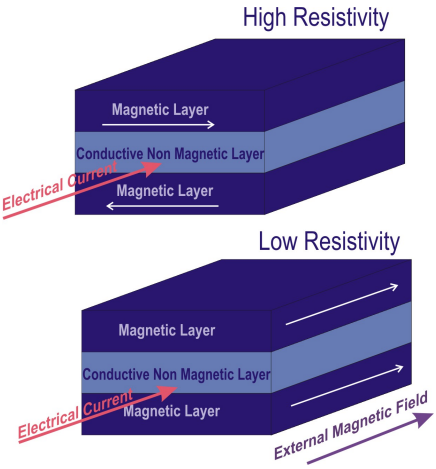

Fig. 2. GMR working principle scheme

The effect was first described in 1988 but in the time until 2005, the GMR commercial devices have been used mostly as magnetic encoders and switches, and very much related to the field of magnetic recording. There was not a significant manufacture of sensors. Among the 47 companies we bench-marked manufacturing magnetic devices: sensors, reed switches, encoders, etc (Table 1), it was only possible to find suitable magnetic sensors for geomagnetic mapping in NVE and Hitachi Metals.

Table 1. Companies manufacturing magnetic sensors

Companies commercializing magnetic sensors (2005)				
N.	**ENTERPRISE**	**WEB**	**PRODUCTS**	
			SENSOR TYPE	**APPLICATION FIELD**
1	Allegro	www.allegromicro.com/Products.aspx	HALL EFFECT	Currrent Sensors Magnetic speed sensors Magnetic Digital Position Sensors Engine speed sensing Electronic Power Steering (EPS) Fan and pump systems Infotainment Lighting systems Hybrid/Electric vehicles
2	Analog Devices	www.analog.com/en/index.html	HALL EFFECT	Automotive Throttle Position Sensing Pedal Position Sensing Suspension Position Sensing Valve Position Sensing Industrial Absolute Position Sensing Proximity Sensing
3	Asahi Kasei Electronics	www.asahi-kasei.co.jp/ake/en/	HALL EFFECT MR	One chip pulse encoder IC Programmable linear Hall effect IC for one axis position detection Non-contact rotation angle sensor
4	Ascension Technology	www.ascension-tech.com/	Third-generation pulsed-DC magnetic tracking technology	Surgical Navigation and Image Guided Procedures Biomechanics & Ergonomics Simulation & Training Real-time Visualization & Virtual Reality 3D Animation & Live Performance
5	Asonik	www.asonik.eu/	HALL EFFECT	Electro Cardio Recorder Computerized Cavendish Balance Multiresonance minispectrometer type NEQ-5

Table 1. (*continued*)

Companies commercializing magnetic sensors (2005)				
N.	ENTERPRISE	WEB	PRODUCTS	
			SENSOR TYPE	APPLICATION FIELD
6	Bartington	www.bartington.com/	Fluxgate	Defence: Marine Defence: Land Aerospace Geosciences Near Surface Geophysics Physics Medical Industrial
7	Baumer Electric	www.baumer.com/int-en/homepage/	HALL EFFECT MR	Monitoring of rotational speed Detection of final positions Object detection Indirect fill level detection
8	EMI Technology Center	www.slb.com/about/rd/technology/emi.aspx	Induction	High frequency measurements Marine sensors Magnetotellurics
9	EMX Industries	www.emxinc.com/	HALL EFFECT	Proximity Sensors
10	ETS lindgren	www.ets-lindgren.com/	Magnetic Resonance Imaging Shielding	Magnetic Resonance Imaging Equipment
11	F.W. Bell	fwbell.com/default.aspx	HALL EFFECT MR	Laboratory Instrumentation
12	Fischer Custom Communications	www.fischercc.com/	Induction	Emissions detection
13	Group3 Technology	www.group3technology.com/	HALL EFFECT	Control Systems
14	Hitachi Metals America	www.hitachimetals.com/	GMR	Wind Power Energy

Table 1. (*continued*)

Companies commercializing magnetic sensors (2005)				
N.	**ENTERPRISE**	**WEB**	**PRODUCTS**	
			SENSOR TYPE	**APPLICATION FIELD**
15	HL Planartechnik	www.meas-spec.com/hl-planartechnik.aspx	MR	Position sensors Rotary displacement sensors
16	Honeywell	honeywell.com/Pages/Home.aspx	MR	Navigation systems Aerospace
17	IC Haus	www.ichaus.de/	HALL EFFECT	Encoder
18	IFM efector	www.ifm.com/ifmus/web/home.htm	Induction	Food and Beverage Applications
19	Infineon	www.infineon.com/cms/en/product/index.html	HALL EFFECT	Automotive Industry Consumer applications
20	Infra	infra-electronic-sensors.blogspot.com.es/	Induction	Position sensors Rotary sensors
21	Lake Shore Cryotronics	www.lakeshore.com/Pages/Home.aspx	HALL EFFECT Induction Fluxmeter	VSM, Cryogenic applications
22	Less EMF	www.lessemf.com/	HALL EFFECT	AC and DC meteres
23	Magnetic Instrumentation	www.maginst.com/	Induction HALL EFFECT Fluxgate	
24	Magnetic Physics	www.magnet-physics.com/	Induction HALL EFFECT	Laboratory Instrumentation
25	Magnetic Sensor Corporation	www.magsensors.com/	Induction	VR Speed Sensor Electromagnets Solenoids Motors IR Steering Mirrors
26	Micronas	www.micronas.com/en/home/index.html	HALL EFFECT	Automotive

Table 1. (*continued*)

Companies commercializing magnetic sensors (2005)				
N.	ENTERPRISE	WEB	PRODUCTS	
			SENSOR TYPE	APPLICATION FIELD
27	Nanjing New Zhongxu Microelectronics	www.zhongxu.com/english/index.asp	HALL EFFECT	
28	NVE	www.nve.com/index.php	GMR	Medical Sensors Gear Tooth Sensors
29	Ohio Semitronic	https://www.ohiosemitronics.com/	HALL EFFECT	Magnetic Field Sensing applications
30	Philips	www.philips.com	AMR	Compas Position sensor
31	PNI	www.pnicorp.com/	Induction	Military applications Scientific applications Robotic Mobile & Tablet Gaming
32	Polatomic Inc	polatomic.com/	Laser-pumped helium	UAVs and Helicopters Underwater Space / Planetary
33	Prodyn Technologies	prodyntech.com	Induction	
34	Quasar Federal Systems	www.quasarfs.com/	Induction	Geophysical Exploration Defense
35	Rikei	www.rikei.com/en/index.html	MR	Mobile Phone PDA
36	RMS Instruments	www.rmsinst.com/	VLF (Very Low Frequency)	Geophysical
37	Samsung Electro Mechanics	www.samsungsem.com/index.jsp	HALL EFFECT	Mobile communication devices

Table 1. (*continued*)

Companies commercializing magnetic sensors (2005)				
N.	**ENTERPRISE**	**WEB**	**PRODUCTS**	
			SENSOR TYPE	**APPLICATION FIELD**
38	Sensitec	www.sensitec.com/en/?s=	MR	Angle, Length, Current and Magnetic field measurement
39	Senstronic	www.senstronic.com/	Induction MR HALL EFFECT	Proximity sensors
40	Tel Atomic	www.telatomic.com/	NMR HALL EFFECT	NMR equipment Magnetic Field Measurement
41	Ultra Electronis PMES	www.ultra-electronics.com/	Induction	AC magnetic signals Magnetic Signatures Measuring and degaussing systems
42	Xensor Inc	www.xensor.com/	Induction MR HALL EFFECT	Magnetic sensors
43	Xushi	www.xushi-sensor.com/	HALL EFFECT Reed switches	Position sensors and valves for industrial equipments and automated pipelines in plastic, light industry, shoemaking, textile, chemical industry, petroleum, tobacco, food, metallurgy
44	Zetex	www.diodes.com/	MR HALL EFFECT	Switches (Unipolar and Omnipolar) Bipolar latches (Single Output and Complementary Output) Smart Fan Driver
45	AnaChip	www.chipdocs.com/manufacturers/ANACH.html	HALL EFFECT AMR Non Volatil Memory	Distributor
46	GMW Associates	www.gmw.com/	HALL EFFECT Induction Fluxgate	Distributor and integrator
47	Sensor Solutions	www.sensorsolutions.biz/	Sensors technologies (not magnetic)	Capable to work in high magnetic fields (7T)

The candidate COTS for the mission are limited to those listed in Table 2. Actually the gradiometers are purchased to complement the measurement of the magnetic field with a measurement of the gradient.

Table 2. List of initial candidates for GMR COTS sensors

Item	Reference	Characteristics	Manufacturer
1	HM55B	GMR Magnetic Sensor	Hitachi
2	AA002-02	GMR Magnetic Sensor	NVE
3	AA005-02	GMR Magnetic Sensor	NVE
4	AAH002-02	GMR Magnetic Sensor	NVE
5	AAL002-02	GMR Magnetic Sensor	NVE
6	AB001-02	GMR Gradiometer	NVE
7	ABH001-00	GMR Gradiometer	NVE
8	AAV001-11	Spin Valve Magnetic Sensor	NVE
9	AAV002-11	Spin Valve Magnetic Sensor	NVE

Among the COTS firstly taken into consideration: sensors by Hitachi and NVE, it was decided to focus on the NVE sensors because the Hitachi sensors are explicitly not recommended for radiation proof [15].

The former devices under test were the magnetic sensors AA002, AAH002 and AAL002 and the gradiometers AB00102 and ABH001-00 of NVE [16]. The selection was based on their higher sensitivity compared to other sensors of the same families and the appropriateness of the dynamic range. For instance, AA005 has a significant higher dynamic range between 1 and 7 mT, above the specifications of the mission.

GMR magnetic sensors have an active area of approximately 350 microns by 1400 microns. The sensors are configured as a Wheatstone bridge with resistors of 5 kΩ made of GMR material. The sensors are provided with flux concentrators for two purposes: to provide the Wheatstone bridge with an asymmetry that unbalances the output of the Wheatstone bridge due to the different shielding of the resistors and to tailor the sensitivity.

The formula NVE provides for the calculation of the field in the position of the sensors due to the effect of the flux concentrators (FC) is:

$$B_{sensor} = 60\% \frac{l_{FC}}{g_{FC}} B_{applied} \tag{1}$$

where l_{FC} (~ 400 μm) is the length of the flux concentrators and g_{FC} (~ 100 μm) the gap between them.

As a result these sensors create an artificial field gradient in the chip by means of which the magnetic field is measured.

In NVE magnetic gradiometers the flux concentrators are removed so the Wheatstone bridge has zero output in the presence of a uniform magnetic field all along the dimensions of the chip. In contrast the output is unbalanced in the presence of a gradient field being the shift in voltage proportional to the field and to the spacing between pairs of resistors (0.3 mm, 0.5 mm, or 1.0 mm depending on the sensor product). As it has been mentioned, these sensors were purchased in case that a complementary measurement could be performed, mostly motivated by the presence of a nearby dipole, since OPTOS has not a magnetic cleanliness program. This option was later discarded.

Finally a couple of spin valve sensors were purchased for comparison but they were not used for this project, so from now on this work will focus on the magnetic sensors.

Characteristics of the purchased sensors can be seen in Table 3.

When comparing with AMR sensors, GMR are more efficient in terms of sensitivity per voltage. Also the power consumption of GMRs is lower due to the higher resistance (5 kΩ compared to a 1 kΩ typical value of AMR.

Table 3. Characteristics of AA002, AAH002 and AAL002 sensors [16]

Parameter	Sensor type			Unit
	AA002	AAH002	AAL002	
Electrical resistance	5	2	5.5	kΩ
Sensitivity	[30, 42]	[110, 180]	[30, 42]	mV / V mT
Saturation Field	1.5	0.6	1.5	mT
Bridge Voltage Range	[<1, 24]	[<1, 24]	[<1, ±25]	V
Operating Frequency	[DC, > 1]	[DC, > 1]	[DC, > 1]	MHz
Operating Temperature Range	[-50, 125]	[-50, 150]	[-50, 150]	ºC
Bridge Electrical Offset	[-4, +4]	[-5, +5]	[-4, +4]	mV / V
Signal Output at Maximum Field	60	40	45	mV / V
Linear Range	[0.15, 1.05]	[0.06, 0.30]	[0.15, 1.05]	mT
Nonlinearity	2	4	2	% (unipolar)
Hysteresis	4	15	4	% (unipolar)
Tempco of Resistance	0.14	0.11	0.11	% / ºC
Tempco of Output at Constant supply Current	0.03	0.1	-0,28	% / ºC
Tempco of Output at Constant supply Voltage	-0,1	0	-0,4	% / ºC
Off Axis Characteristic	Cos β	Cos β	Cos β	β angle between field and sensitivity axis
ESD Tolerance	400	400	400	V pin-to-pin HBM

Figure 3 shows the response curves of the candidate sensors. Two characteristics should be remarked: one is that GMR is an even effect and thus their response is the same no matter the direction of the field and the other is that response curves present a not negligible hysteresis.

The transition from the ordered saturated magnetized state up to the high resistance state goes through a line with higher sensitivity while the transition from the spontaneous alternated magnetization towards the saturation magnetized state goes through a lower sensitivity curve. In the low field region, the repeatability is really poor. However the sensitivity of any of the branches is very good and appropriate for the magnitude of the Earth magnetic field intensity.

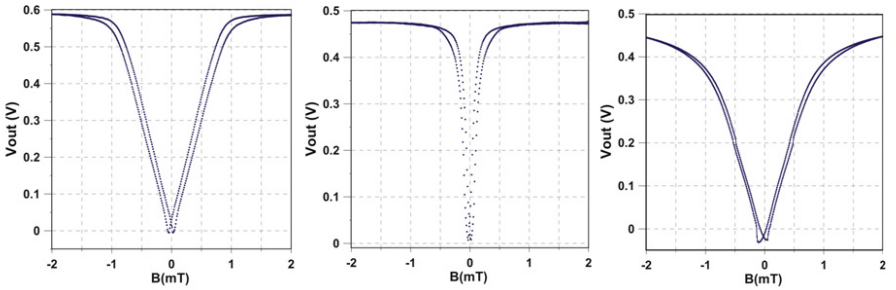

Fig. 3. AA002, AAH002 and AAL002 response curves for a 2 mT range

Another issue (mentioned in) is the high dependence of GMR sensors with temperature. Figure 4 corresponds to a sequence of measurements of the AAL002 device performed at a fast rate, while the sensor is being warmed up by means of a close electrical resistor (Joule effect). It can be seen how the sensitivity of the sensor decreases monotonically with the increase of temperature. This characteristic will have to be taken into account in two aspects: on the first hand a thermal compensation will be essential, and on the other hand, any coil for the correction of the previously mentioned odd response will have to be placed at a certain distance from the sensor to avoid direct heating.

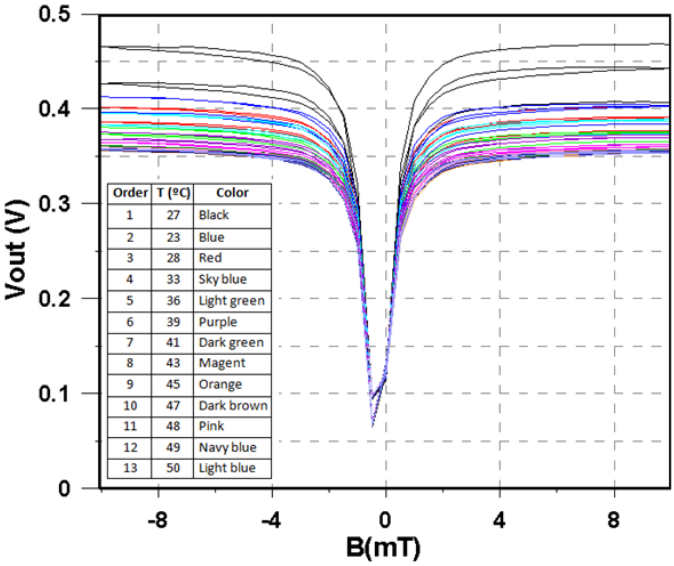

Fig. 4. Degradation of the response of the AAL002 magnetic sensor as the temperature increases

The next step is to study the linearity of the different candidates to discern which the most suitable working region is and with which sensor.

The response of the GMR sensors under study is not linear in the whole range. Though this actually can be compensated calibrating the curve, for basic applications with simple proximity electronic and data processing it is much more convenient to have a linear response.

To study where the sensor is linear attention is paid to the first derivative of the output response respect the external magnetic field (denoted by dVout/dB in the graphs). When the value of the derivative is constant, i.e. the sensitivity is constant, the sensor is considered to have a linear response. The ideal situation is that both branches of the hysteresis loop had the same slope and thus, the same sensitivity and that the linearity is a maximum.

To study this, a simple set up is developed (Figure 5). A MATLAB program controls the intensity of a power source (E3631E by Agilent Technologies) that supplies with current a coil setting the external magnetic field. The direction of the current is changed by means of two relays connected to the switches of the Data Acquisition / Switch Unit (HP 34970). The value of the electrical current is requested to calculate the magnetic field. The output signal of the sensor is acquired by the Data Acquisition / Switch Unit.

Each measurement consists of the average of only two samples. These first tests are performed at very low frequencies to get the external field completely stabilized.

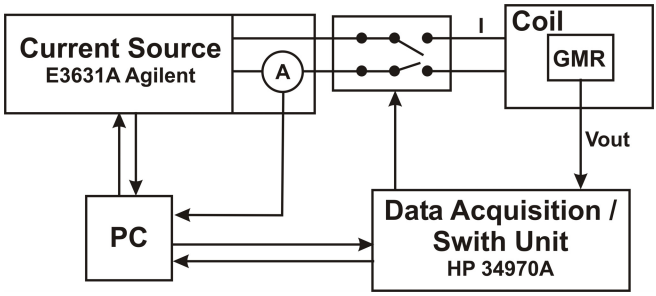

Fig. 5. Block diagram of the set up for the measurements

The coil used is not a perfect Helmholtz one and the area of homogeneous magnetic field is confined in a region of 5 mm with an homogeneity better than $9 \cdot 10^{-2}$ %. A mechanical fixture is manufactured to guarantee the repeatability in the positioning of the sensors.

Figures 6, 7 and 8 show the response curve (dark blue referenced to the left hand side Y axis) and the derivative / sensitivity (light blue referenced to the right hand Y axis) of the AA002 , AAH002 and AAL002 respectively when a ramp of ± 2 mT is applied.

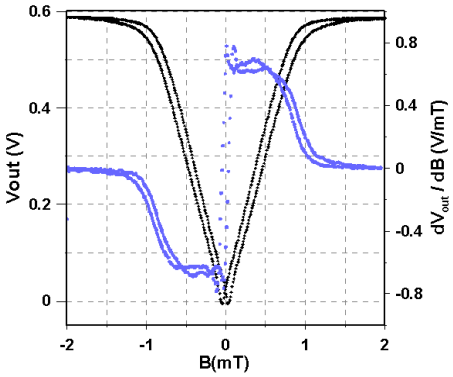

Fig. 6. Response curve and derivative of the AA002 sensor vs. the external magnetic field

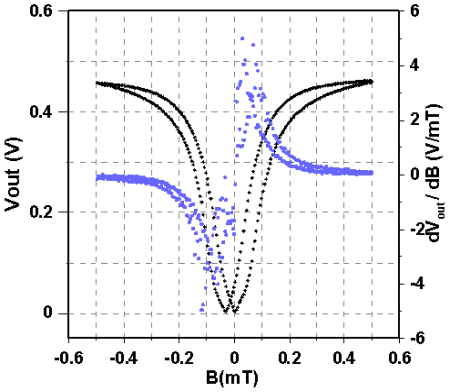

Fig. 7. Response curve and derivative of the AAH002 sensor vs. the external magnetic field

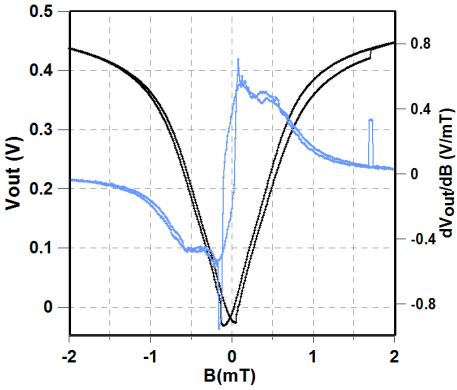

Fig. 8. Response curve and derivative of the AAH002 sensor vs. the external magnetic field

At a glance it can be seen that AA002 and AAH002 show higher hysteresis than AAL002, and the linearity is better in AAH002 and AAL002.

Regarding the derivative of the field (sensitivity) AAH002 sensor (Figure 7) does not even present a linear interval in the field range. This sensor is discarded for the in flight experiment.

However, AA002 and AAL002 derivatives are constant for a certain interval of the field (~0.5 mT). In the sensor AA002 the derivative is split into two branches due to the hysteretic behaviour of this sensor while in the AAL002 the split is minimal. Actually, the dispersion of the derivative in the two branches is higher in the AA002 than in the AAL002.

Following this argument of a less hysteretic and a more linear response, AAL002 sensor is selected for the OPTOS experiment.

3 Biasing Mechanism

Previously it has been discussed the even nature of the GMR effect, which for practical purposes limits the capability of the sensors to measure the magnitude of the field but not the direction. Other magnetoresistive sensors have this problem as well but even at commercial level, the devices are provided with a biasing mechanism called Barber pole. In these sensors the magnetic material (a monolayer) has a set of copper microstraps inserted at an angle of 45º of the magnetic strap making the current pass through the material at an angle of -45º following the shortest distance between better conductive layers. Also the devices have a microcoil assembled so a magnetization in the easy axis can be performed. In such conditions, when a magnetic field with a component perpendicular to the easy axis is applied, the magnetization rotates to an equilibrium position between the action of the field and the previous state magnetized in the easy axis [17]. With this mechanism, AMR devices are sensitive to field direction since the projection of the magnetization on the direction of the current is different for both signs of the field.

More recently, it has been reported the use of crossed axis GMR for odd response as a function of the field [18], which has been recommended for linear applications without excitation. However, available COTS GMR sensors in 2005 are not provided with such a mechanism and thus, external biasing needs to be performed to measure the vector field [20-24]. In this subchapter this mechanism is introduced.

The first step for biasing is to find an optimum working point. It has been described that the zero field area is a very poor area for measuring so biasing fields are applied to find a better working area. Figure 9 shows biased curves for AAL002.

The mechanism proposed to solve the hysteresis problem is the following. If both branches are characterized it is possible to measure with the sensor in any of them but what is more, if it is possible to locate the magnetic sensor in one of the branches, the measuring procedure is easier and the repeatability higher.

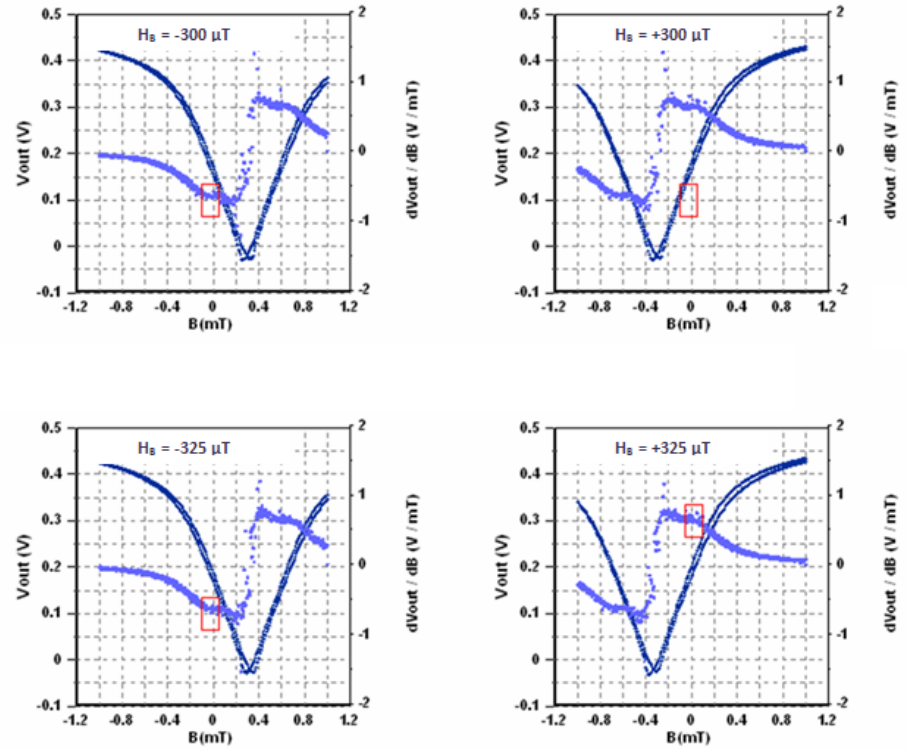

Fig. 9. Response curve (dark blue referred to the left hand side Y axis) and derivative (light blue referred to the right hand side Y axis) of the AAL002 sensor vs. the external magnetic field. For different bias field in both senses.

This is the goal of this mechanism: to apply a magnetic field high enough so as to guarantee that the sensor is following a certain branch when this field ceases.

In Figure 10 it is shown a graph of the response (dark blue) of the AA002 and its derivative (light blue) in a range of field of ± 2 mT. It has been used the AA002 curve because it is the one which shows the higher hysteresis and it is easier to distinguish between the branches.

In the absence of an external bias and S / R magnetic field (State 1), the response of the sensor is very uncertain and highly dependent of the previous states.

If a bias field is applied (State 2) there are two possible states depending on the previous state of the sensor. If the environment is relatively clean, the most probable branch is the one on the left in the upper part of Figure 10, this is, the one with less sensitivity. To avoid this uncertainty around the working point a Set field, with a higher value of that of the biasing field is applied (State 3) followed by a bias field centred in the range of constant derivative (State 4). In this way the sensor goes to this 4^{th} state from state 3 through the most sensitive path.

In the negative part of the measurement, the procedure is exactly the same. The State 5 is uncertain but after the Reset pulse (State 6), the State 7 is already defined and the corresponding sensitivity characterized.

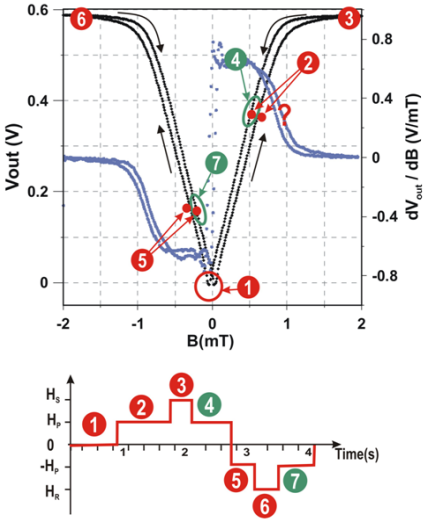

Fig. 10. Set Reset mechanism. Correspondence between the field applied and the magnetic state of the GMR multilayer

The result of this procedure for different values of the S / R field is shown in Figures 11 and 12.

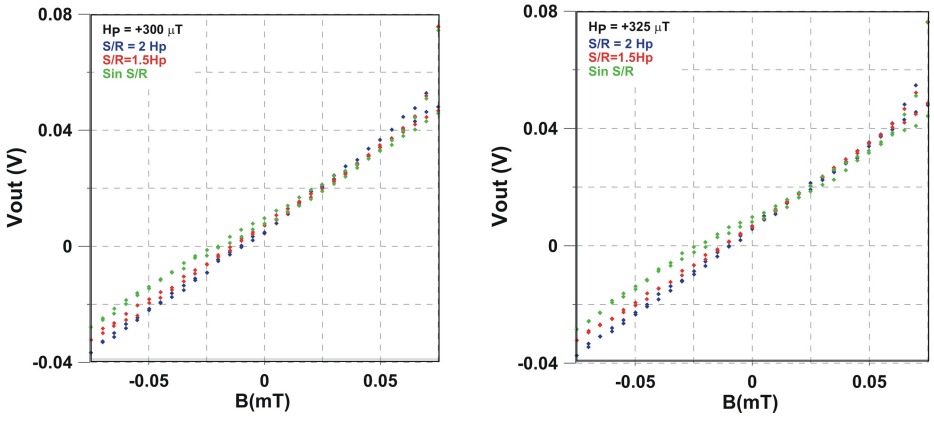

Fig. 11. Response of the AA002 sensor with the bias field mechanism (green), with a 1.5 times the bias field Set / Reset Field (red) and with two times the bias field Set / Reset field (blue)

It can be seen in these figures that the higher the S / R field the higher sensitivity. Also at the appropriate value of the bias field the derivative has the less dispersion.

The Set Reset mechanism together with the alternating bias improves notably the behaviour of the sensors being the best choice the AAL002, which presents the less hysteretic behaviour and thus the higher repeatability. The value of the bias field is around 300 and 325 μT and the minimum detectable field is now limited by the power sources used.

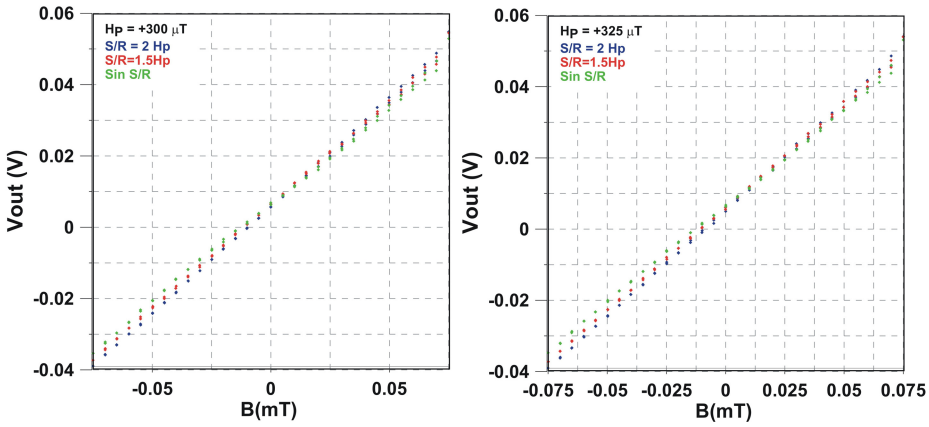

Fig. 12. Response of the AAL002 sensor with the bias field mechanism (green), with a 1.5 times the bias field Set / Reset Field (red) and with two times the bias field Set / Reset field (blue)

4 Qualification of the Sensor

As it has been explained, GMR sensors were in a commercial stage of development, thus the technology readiness level (TRL) attributable to the COTS sensors was around 4 following the NASA and ESA standards.

For OPTOS mission the qualification of the sensor for flight use was performed by means of three different tests:

- An outgassing test to check the suitability of the plastic package
- An irradiation test with protons to discard a malfunction of the sensors under radiation (potential creation of defects of the material, and thus in the magnetic response)
- Tailored upscreening for the mission

OUTGASSING

Space environment is often thought as vacuum. In this atmosphere, components can outgas. This implies mainly three concerns:

- Their operational properties can change giving rise to dimensional stability and lubrication problems for instance
- They can generate a "gas cloud", which can perturb measurements specially in scientific missions
- The "gas cloud" can condensate on surfaces modifying their operational properties: thermo-optical, radiation effects and electrical with the corresponding thermal and electrical problems

Thus, an outgassing test was performed following the ECSS-Q-70-02 norm from the European Space Agency "Thermal vacuum outgassing test for the screening of space materials". The purpose of this test is to ascertain if the package of the sensor outgases by means of the measurement of the:

- Total mass loss (TML)
- Returned mass loss (RML)
- Collected volatile condensable material (CVCM)

This test was performed at INTA. GMR sensors showed a negligible outgassing, and thus, no expected change in operational properties of the plastic package, neither do "gas cloud" emission or condensation, add derived problems. As a result, the package was considered apt for flight in terms of outgassing.

IRRADIATION

Satellites orbiting the Earth have a very different weather than equipment on the surface. "Space vacuum" involves plasmas, all range of energies electrons and ions, which potentially can damage the equipment of the spacecrafts. High energy particles (10 MeV) have the potential to ionize atoms in the materials through which they propagate and low enery particles (< 100 eV) they can produce accumulation of charge or other types of materials degradation.

At this point it is very difficult not only to simulate the interaction between these particles and the materials with experiments but also it is difficult to estimate the radiation environment of the missions because of the changing nature of the space weather. But one normal way of operation in space missions is on the first hand to generate an envelope of radiation for the mission life and on the other hand, to perform radiation tests generally with gamma and with protons to simulate the different damages as a function of their energy.

In our case an exhaustive campaign of gamma irradiation for anisotropic magnetoresistive (AMR) sensors had been performed for the sensors of NANOSAT-01, launched in 2004. Even though GMR and AMR technologies are not the same, it was assumed that the magnetic material was immune to the total irradiation dose up to tens of krad Si and consequently, a campaign of irradiation with protons was performed, to study the effects the high energy particles could have on the sensing properties of the devices.

At the time of the irradiation campaign the number of sensors for flight was limited and some of them had been reserved for the rest of the qualification process, so a further assumption was made: that all NVE magnetic sensors have similar materials

and the possible damages will be homogeneous in all of them. Under this assumption, sensors of the type AA003 underwent the proton irradiation campaign.

The tests were performed in the RADEF facility, located in the Accelerator Laboratory at the University of Jyväskylä, Finland (JYFL). The facility includes a beam line dedicated to proton irradiation studies of semiconductor materials and devices.

The real fluence received by the GMR sensors is listed in Table 4.

Table 4. Mean Fluence and standard deviation (protons / cm^2) for the irradiated devices

Step	Fluence ($p+/cm^2$)	Std. Dev. ($p+/cm^2$)
0	0	0
1	8,00E+10	4,27E+09
2	4,80E+11	2,56E+10
3	8,80E+11	4,70E+10
4	1,28E+12	6,83E+10
5	1,68E+12	8,97E+10
6	2,08E+12	1,11E+11

The fluence is calculated for a typical satellite in a Low Earth Orbit (LEO).

Four AA003 GMR sensors were exposed to this radiation. The response of the sensors for a magnetic field ramp was measured after each step starting with a saturating magnetic field in one direction and returning to this point to measure changes in sensitivity and hysteresis.

A mechanical set up (Figure 13) was performed to reproduce the position of the sensor in every check.

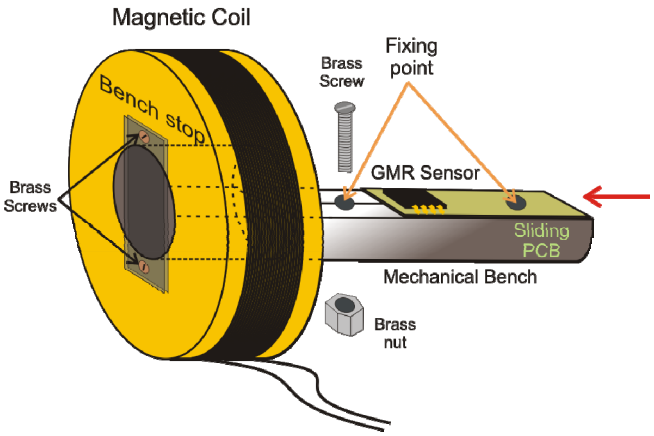

Fig. 13. Mechanical bench for repetitive magnetic characterization of GMRs

The sensors did not show appreciable changes in sensitivity and hysteresis along the irradiation, so they are considered as radiation robust for the fluence and rates used.

TAILORED UPSCREENING

OPTOS is a mission with an expected life time of three years. The components of the missions need to have proven that they can stand the conditions of the life time. To do so, an accelerated ageing of the devices is foreseen. This is called upscreening.

During the upscreening process a representative number of AAL002 GMR devices of the same badge are tested. The sequence of the upscreening, designed by INTA, and the number of components for each step are shown in Figure 14.

After a serialization a visual inspection of the 30 units of the lot is made to ascertain that there are no irregularities in the devices. This step is performed by means of an optical microscope at 10x. Purchased sensors did not present any visible non conformity.

For the following steps, the sensors are placed in a PCB with appropriate sockets inside a magnetic shielding chamber with a coil (Figure 15) to permit the checking of the magnetic characteristics of the sensors in the different conditions. The whole set up is placed in the thermal chambers for the qualification process.

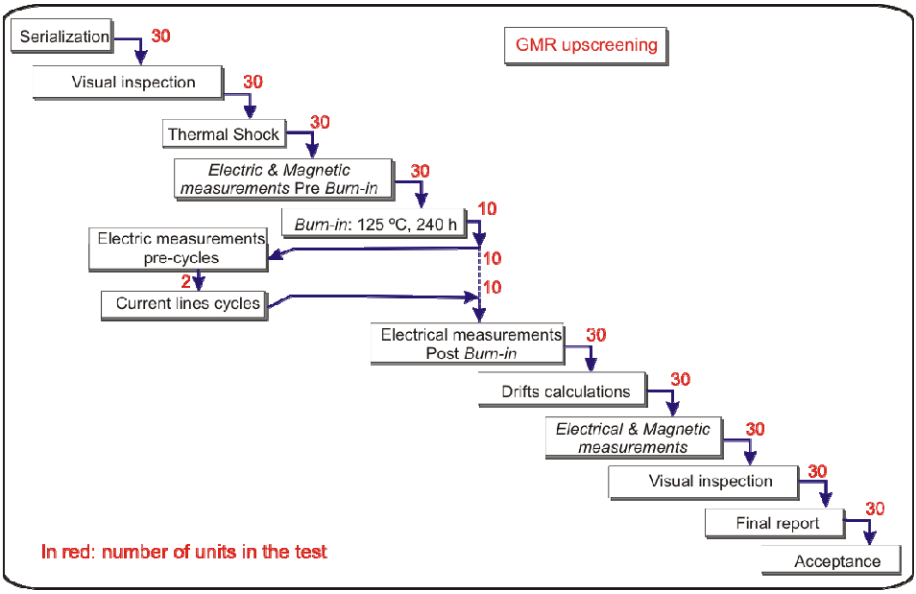

Fig. 14. Tailored upscreening for GMR sensors

Fig. 15. PCB with sockets inside the one-layer mumetal shielding chamber

The following step is a thermal shock which is performed to determine the resistance of the part to sudden changes in temperature. The parts undergo a specified number of cycles, which start at room temperature. The parts are then exposed to the highest qualification temperature (+70ºC) and, within a short period of time, exposed to the lowest qualification temperature (-20ºC), before going back to room temperature. After the final cycle, external visual examination of the package, pins, and seals is performed at 10x. The marking is also inspected (magnification lower than 3x). As no illegible mark and/or or evidence of damage to the package, pins, or seals after the stress test was noticed, the devices are apt to continue the burn-in test, in which the temperature is risen to 125ºC for a long time. In contrast to the specified time of 240 hours the devices remained at 125ºC for 92 hours, which was agreed by the system engineer.

At this point it is checked the electrical and magnetic response of the devices, i.e. the measurement of the Wheatstone bridge resistance (not powered) and a five points ramp of magnetic field generated by means of an external coil.

Devices showed a negligible deviation of their electrical Wheatstone bridges resistors (lower than 100 ppm) and the sensitivity measured does not change appreciably (~1 % outside the magnetic shielding chamber).

The next step is the whole life simulation of the devices. This consists in a non stop operation of the sensors at an accelerated rate of excitation to age the components.

Since the simulation of the mission life cycle is potentially stressing for the components, only a small amount of the devices undergo this proof.

After this test the resistance of the components is measured with no observed deviation respect to the former measurements.

The calculation of the drifts resulted in a negligible deviation of the response of the sensors with magnetic field (~1 % outside the magnetic shielding chamber) and no observable variation of the Wheatstone bridges electrical resistances (lower than 100 ppm). Thus, AAL002 GMR sensors are considered qualified for OPTOS mission.

5 Design of the Device

In this section it is explained the mechanical design of the sensor. The description of the front end electronics are out of the scope of this chapter.

AAL002 GMR sensors are one axis sensor. To develop a vector magnetometer they need to be located in perpendicular planes. A cube of FR4 material was used for this purpose (Figure 16).

The cube was mechanized with some slots for the biasing mechanism, which consists in magnetic coils wounded around each magnetometer producing a biasing field in the sensing direction. The field needs to be high enough to saturate the GMR sensor (in the order of 600 μT).

The biasing mechanism permits the measurement of the field with its direction. To do so, attention needs to be paid in the winding of the coils around each sensor for a right handed system aligned with the reference system of the spacecraft.

Since only four of the pins of each magnetometer need to be connected, no printed circuit board was performed. The connection of the pins was wired.

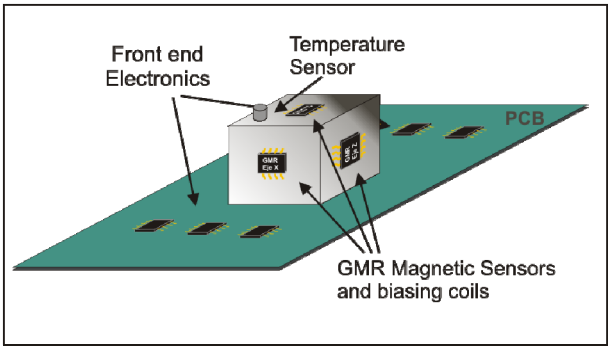

Fig. 16. Scheme of the FR4 cube with three orthogonal GMR devices

Figure 17 shows a picture of the GMR flight model. Towards the centre it can be seen the cube with the three GMR sensors and their biasing windings.

The whole PCB consists in the GMR sensor, the optical link and the corresponding adapter. The dimensions of the PCB are 89 mm, 78.8 mm ad 19 mm and the nominal power is lower than 500 mW.

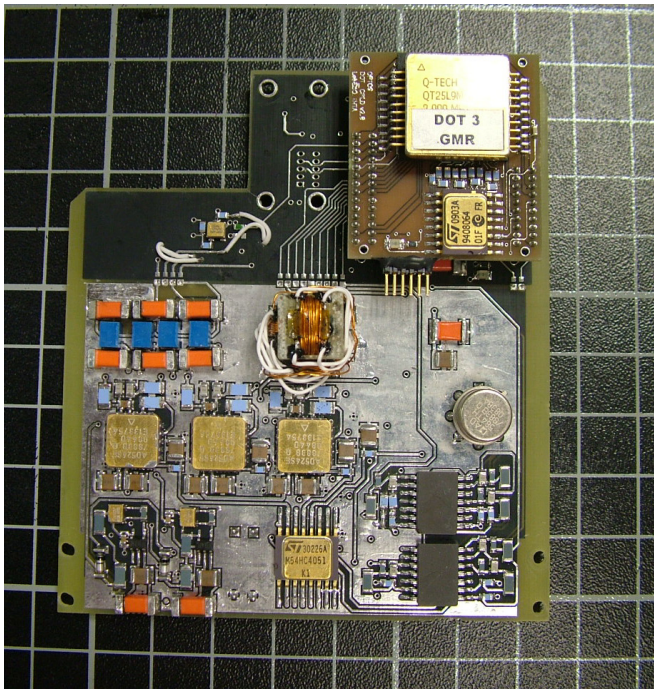

Fig. 17. Flight model of the GMR based vector magnetometer

6 Performance

GMR sensor for OPTOS is a vector magnetometer with a dynamic range of ± 150 μT in every component. The sensitivity of the different axes is: 28 mV/ μT – X axis, 24 mV/ μT – Y axis ad 17 mV/ μT - Z axis.

The offsets in the different axes: -115 mV (X axis) , -105 mV (Y axis) and -124 mV (Z axis), though this offset will have to be in flight calibrated due to the proximity to magnetic materials.

The stability of the sensor is fairly good (better than 500 ppm in one hour) and the cross axis is less than 1 %. Sensors still need a final calibration with temperature.

GMR sensors have higher sensitivity than other magnetoresistive sensors (AMR) but their intrinsic noise, likely due to their more complicated structure, is higher and implies a higher low-field detectivity limit. Due to the ultimate performance-limiting factor of the noise in GMR sensors, it is worthy to devote some effort in the determination of it and in the understanding of the noise sources. Besides, the measurement of the power spectral density – PSD, can give any clue of the better operation frequency of the sensor.

In the low-frequencies range, the two sources of noise are the white noise or thermal noise and the 1/f noise [25-26].

The former is related with spontaneous fluctuations induced by the thermal excitations and its PSD is given by the Nyquist equation:

$$PSD(f) = 4k_B TR \tag{2}$$

Where "k_B" is the Boltzmann constant, "T" the absolute temperature and "R" the electrical resistance. In our case this noise is lower than 2 pT /√Hz.

This noise is a function exclusively of the resistance (not of the magnetic field), and cannot be suppressed nor modified.

The latter source of noise, the 1/f noise, appears in magnetic and non magnetic systems and it is related to fluctuations of energy around equilibrium. Its PSD, given by Hooge in 1969, corresponds to:

$$PSD(f) = \frac{\gamma_H V^2}{N_C f} \tag{3}$$

Where "γ_H" is the Hooge´s constant, "V" the applied voltage and "N_C" the number of charge carriers in the active volume.

This noise is inversely proportional to the volume so it becomes dominant in small structures.

The set up for the measurement of the PSD in the GMR AAL002 sensor is depicted in Figure 18.

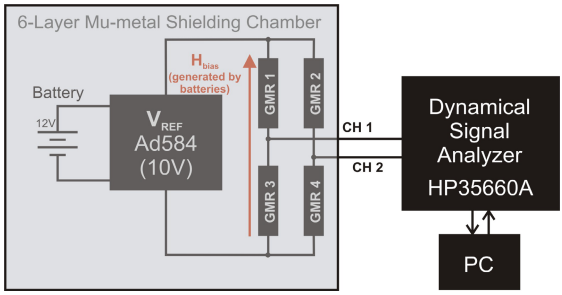

Fig. 18. Set up for the measurement of the PSD of the GMR AAL002 magnetic sensor

The sensor is supplied with 10 V by means of a voltage reference AD584 supplied with batteries. The coils to provide the bias field are also supplied with batteries. The bridge configuration has the advantage that voltage fluctuations will appear on both signal lines and thus, they will be able to be subtracted. To reduce as much as possible the unwanted pickup of external magnetic field fluctuations due to both the noise in the bias field or the environmental noise, the Helmholtz coils generating the bias field are high enough so as to avoid magnetic gradients in the region of the magnetic sensor and the battery voltage is monitored not permitting a voltage drop higher than a 0.1 %. Finally, the whole system is isolated from external fluctuations of the magnetic field by means of a 6 layer mu–metal shielding structure.

There is no pre-amplification of the magnetic sensor signals because the signal analyzer used has input impedance higher than 1 MΩ.

The dynamical signal analyzer is PC controlled to measure the PSD of the two individual channels from DC up to 10 kHz in intervals of 200 Hz with a LabView programme.

Afterwards the two channels are cross-correlated (Figure 19).

The graphs of the noise density are in Volts. The sensitivity is in the order of 300 – 450 mV/mT, so the magnetic noise density at 1 Hz is in the order of tens of nT√Hz and at 1 kHz in the order of nT√Hz.

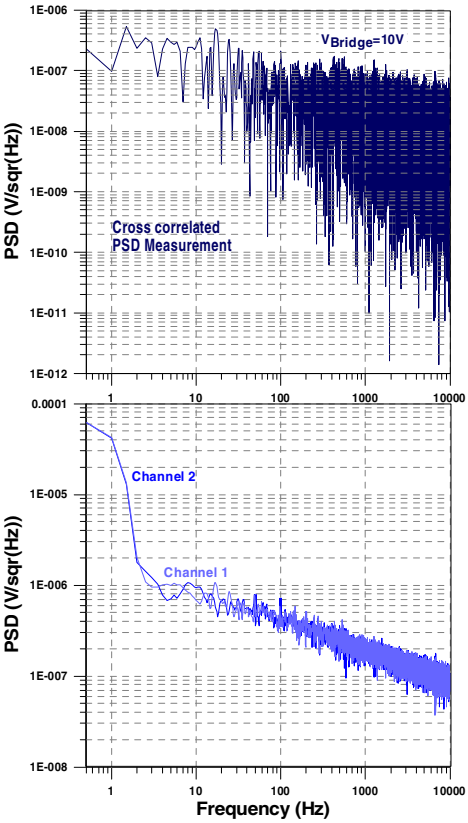

Fig. 19. Cross-correlation (upper graph) of the measurement of the PSD in the two branches of an AAL002 magnetic sensor (graph in the bottom)

The fast decay of the PSD with the frequency together with the suitability of the S / R and biasing mechanism suggest an operation in the range of the kHz instead of a DC operation in which the external magnetic field supposes a modulating signal to the excitation alternating bias field and measure by means of a lock in amplifier.

7 Summary and Conclusions

Working in space conditions is always a challenge; due to the extreme conditions of temperature, radiation and vacuum. This gets even more complicated when one tries to use commercial devices, not thought from scratch to work in space.

The process overviewed in this chapter shows how it was faced the use of commercial giant magnetoresistive devices for flight conditions. The procedure for the qualification of a GMR COTS based vector magnetometer from the definition of the mission and payloads on board to the pre-flight calibrations prior to final assembly and launch is a critical procedure.

The first part of the procedure consists in a bench mark of the enterprises manufacturing magnetic sensors in search of GMR candidates. As a result, it was concluded that the GMR COTS sensor candidate for the fight demonstration is AAL002 by NVE to be onboard OPTOS picosatellite.

A biasing mechanism was designed to the measurement of the field direction. To do so, extra magnetic coils had to be foreseen for the sensors.

The whole qualification process of the COTS sensors has been described: outgassing, irradiation with protons and upscreening. AAL002 sensors seem not to be damaged in the qualification process so they are selected for flight.

Finally the outcome sensor has been fully characterized and characteristics are explained.

In conclusion, GMR COTS sensors present a high dynamical range and high sensitivity (up to 40 mV / V / mT) but they present some disadvantages compared to other magnetic sensors as for instance the lack of linearity, thermal and time stability, repeatability and noise. At this point white noise is negligible and the dominant source of noise is 1/f noise.

This fact makes us think that an excitation of the sensor at frequencies in the order of 1 kHz can lead to a more stable and lower noise operation.

Finally, after all these years of work, OPTOS flight model (Figure 20) is on the bench about to be ready for the launch.

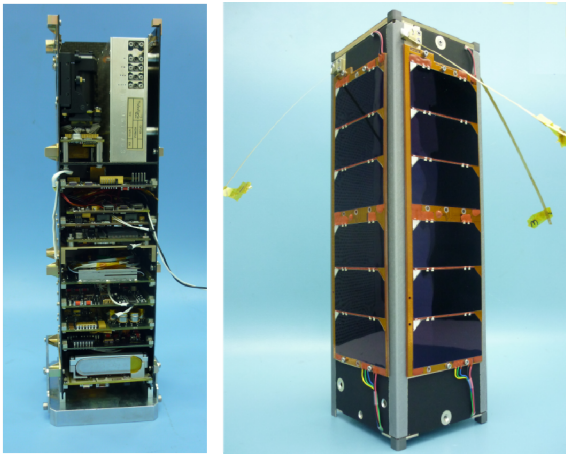

Fig. 20. Current status of OPTOS spacecraft flight model (FM)

GMR COTS roadmap to space can be the fastest ever (Figure 21). Our fingers are crossed for a successful launch and future operation of OPTOS spacecraft, our laboratory is waiting expectantly for the new emerging sensor to qualify. Our hopes are that we have the opportunity to qualify a disruptive technology of magnetic sensing that revolutionizes the space magnetometry.

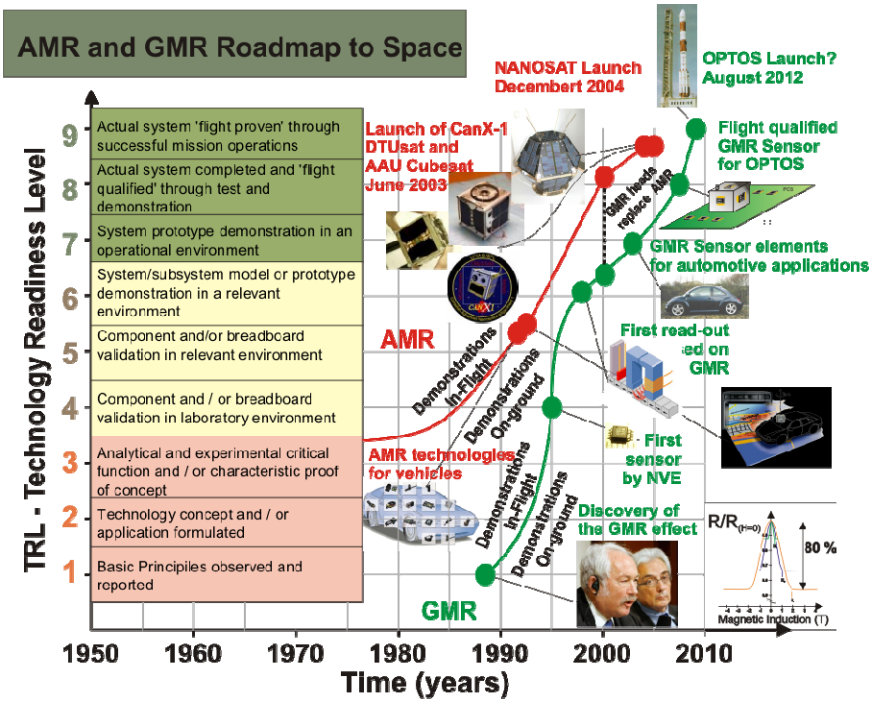

Fig. 21. AMR and GMR roadmaps

Acknowledgements. Author acknowledges OPTOS team for all the support. In particular, OPTOS/GMR team in part supported by MEIGA PROJECT AYA2009 - 14212-C05 -01 / MICINN & AYA2011 -29967-C05 -01 / MINECO and TD02/08 INTA Calvo Rodés grant.

References

[1] Acuña, M.H.: Space-based magnetometers. Review of Scientific Instruments 73(11), 3717 (2002)

[2] Michelena, M.D., Arruego, I., Oter, J.M., Guerrero, H.: COTS-Based Wireless Magnetic Sensor for Small Satellites. IEEE Transactions on Aerospace and Electronic 46, 542–5572 (2010)

[3] Magnes, W., Diaz-Michelena, M.: Future Directions for Magnetic Sensors for Space Applications. IEEE Transactions on Magnetics 45, 4493–4498 (2009)
[4] Michelena, M.D.: Small magnetometers for Space Applications. Sensors 9, 2271–2288 (2009)
[5] Klaassen, K.B., Contreras, J.T.: Thermal transient response of electrical self heating in current-in-plane magnetoresistive heads. IEEE Transactions on Magnetics 42(10), 2438–2440 (2006)
[6] van Peppen, J.C.L., Klaassen, K.B.: A new approach to micromagnetic simulation of thermal magnetic fluctuation noise in magnetoresistive read sensors. IEEE Transactions on Magnetics 42(1), 56–69 (2006)
[7] Maqableh Mazin, M., Liwen, T., Huang, X., et al.: CPP GMR Through Nanowires. IEEE Transactions on Magnetics 48(5), 1744–1750 (2012)
[8] Yupin, S., Pornchai, S., Yoshihiro, O., et al.: Performance Improvement System for Perpendicular Magnetic Recording with Thermal Asperity. IEICE Transactions on Electronics E94C (9), 1472–1478 (2011)
[9] Jia, Z., Misra, R.D.K.: Magnetic sensors for data storage: perspective and future outlook. Materials Technology 26(4), 191–199 (2011)
[10] Aragon, V., Garcia, A., Amaro, R., et al.: OPTOS communications: A high-performance solution. Microwave and Optical Technology Letters 54(4), 943–946 (2012)
[11] Daniel, S., David, K.: A survey and assessment of the capabilities of Cubesats for Earth observation. Acta Astronautica 74, 50–68 (2012)
[12] Tsitas, S.R., Kingston, J.: 6U CubeSat commercial applications. Aeronautical Journal 116(1176), 189–198 (2012)
[13] Najam, A.N., Han, X., Yan, J.L., et al.: An Architecture Analysis of ADCS for Cube Sat: A Recipe for ADCS Design of ICUBE. In: Mechanical and Aerospace Engineering 2012. Applied Mechanics and Materials, vol. 110-116(pts 1-7), pp. 5397–5404 (2012)
[14] Jiménez, J.J., Oter, J.M., Apestigue, V., Hernando, C., Ibarmia, S., Hajdas, W., Sánchez-Páramo, J., Álvarez, M.T., Arruego, I., Guerrero, H.: Proton monitor Las Dos Torres: first intercomparison of in-orbit results. Accepted to IEEE Transaction Nuclear Science, doi:10.1109/TNS.2012.2198241
[15] Magnetic Compass Sensor HM55B Datasheet 19-SM-001-2 p.9 Precaution for use 9.2
[16] NVE Corporation GMR Sensor Catalog, pp.14–19
[17] Caruso, M.J.: Set/Reset Pulse Circuits for Magnetic Sensors. Honeywell Applications Note, AN-201
[18] Freitas, P.P., Ferreira, R., Cardoso, S., Cardoso, F.: Magnetoresistive sensors. J. Phys.: Condens. Matter 19, 165221–165241 (2007)
[19] Reig, C., Cubells-Beltrán, M.-D., Ramírez Muñoz, D.: Magnetic Field Sensors Based onGiant Magnetoresistance (GMR) Tecnology: Applications in Electrical Current Sensing. Sensors 9, 7919–7942 (2009)
[20] Kools, J.C.S., Ruigrok, J.J.M., Postma, B., et al.: Fabrication and characterization of giant magnetoresistive elements with an integrated test coil. IEEE Transactions on Magnetics 33(6), 4513–4521 (1997)
[21] Ripka, P., Tondra, M., Stokes, J., Beech, R.: AC-driven AMR and GMR magnetoresistors. Sens. Actuators A 76, 227–232 (1999)
[22] Vopálenský, M., Ripka, P., Platil, A.: Precise magnetic sensors. Sens. Acuators A 106, 38–42 (2003)

[23] Vopálenský, M., Ripka, P., Kubík, J., Tondra, M.: Improved GMR sensor biasing design. Sens. Acuators A 110, 254–258 (2004)
[24] Dimitropoulos, P.D., Avaristsiotis, J.N.: Integrating the Fluxgate principle in the Spin-Valve and AMR sensor Technologies. Sens. Actuators A 106, 43–47 (2003)
[25] Pannetier, M., Fermon, C., Le Goff, G., Simola, J., Kerr, E., Coey, J.M.D.: Noise in small magnetic systems-applications to very sensitive magnetoresistive sensors2. J. Mag. Mag. Mat. 290-291, 1158–1160 (2005)
[26] Stutzke, N.A., Russek, S.E., Pappas, D.P., Tondra, M.: Low-frequency noise measurements on commercial magnetoresistive magnetic field sensors2. J. Appl. Phys. 97, 10Q107 (2005)